Cyclometallated 2-Phenylpyrimidine Derived Platinum Complexes: Synthesis and Photophysical Properties

Michaela Feckova, Samia Kahlal, Thierry Roisnel, Jean-Yves Saillard, Julien Boixel, Mariia Hruzd, Pascal Le Poul, Sebastien Gauthier, Francoise Robin-Le Guen, Filip Bures, et al.

10.1002/ejic.202100155

Cyclometallated 2-phenylpyrimidine derived platinum complexes : Synthesis and photophysical properties

Michaela Fecková,[a,b] Dr. Samia Kahlal,[a] Dr. Thierry Roisnel,[a] Prof. Jean-Yves Saillard,[a] Dr. Julien Boixel,[a] Mariia Hruzd,[a] Dr. Pascal le Poul,[a] Dr. Sébastien Gauthier,[a] Prof. Françoise Robin-le Guen,[a] Prof. Filip Bureš,*[b] and Dr. Sylvain Achelle*[a]

[a] Univ Rennes, CNRS, Institut des Sciences Chimiques de Rennes - UMR 6226, 35000 Rennes, France.
E-mail: sylvain.achelle@univ-rennes1.fr
https://iscr.univ-rennes1.fr/sylvain-achelle
@chimie_ISCR

[b] Institute of Organic Chemistry and Technology, Faculty of Chemical Technology, University of Pardubice, Studentská 573, Pardubice 53210, Czech Republic.
E-mail: filip.bures@upce.cz
http://bures.upce.cz

TOC

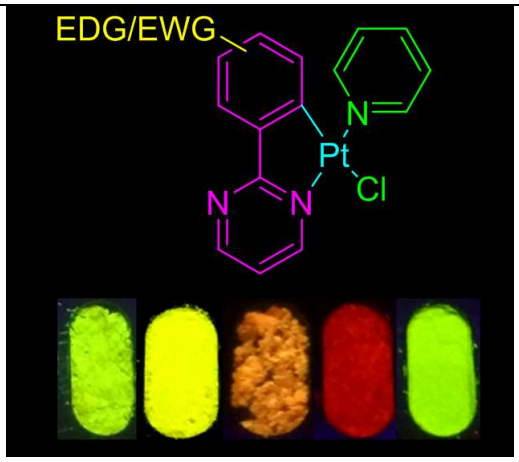

A series of 2-phenylpyrimidine platinum (II) complexes were designed and their phosphorescence properties were studied. The presence of an electron donating group in para position of Pt atom on the phenyl ring significantly increased emission intensity in the solution and lead to a red-shifted phosphorescence in the solid state.

Abstract

A series of five platinum (II) complexes based on 2-phenylpyrimidine ligands have been designed. Pyridine and chloride were used as auxiliary ligands. These complexes exhibit a slightly distorted square-planar geometry. The nature and position of substituent on the phenyl ring was thoroughly studied. The presence of an electron-donating substituent on the phenyl ring in the *para* position of the platinum atom leads to a red shift of the lowest-energy

absorption band, which corresponds to the HOMO→LUMO transition and permits to obtain phosphorescence in deoxygenated CH_2Cl_2 solution. All compounds are emissive in the solid state with a significant redshift for complexes bearing electron-donating substituent on the phenyl ring of phenylpyrimidine ligand.

Keywords : N ligands ; Heterocycles ; Phosphorescence ; Platinum (II) complexes ; Pyrimidine

Introduction

During the past two decades there has been a strong interest in the design of luminescent transition metal complexes.[1] Indeed, these materials exhibit emissive excited triplet states and can be used as emitters for second generation organic light emitting diodes (OLEDs), also called phosphorescent OLEDs (PHOLEDs).[2] In this context, many cyclometallated iridium (III) complexes with N^C 2-phenylpyridine (ppy) type ligands have been developed.[3] Similar phosphorescent Pt(II) complexes have been also designed by various teams,[4] and their emission properties can be tuned by rational ligand modifications.[5] Acetylacetone (acac) is generally used as auxiliary ligand for such complexes.[6] $[Pt(ppy)Cl_2]^-$ complex is known to be not luminescent at room temperature,[5] however it has been shown recently that Pt(II) ppy type complexes bearing chloride and pyridine monodentate ligand exhibit also interesting phosphorescence properties.[7]

It has been also demonstrated that the presence of electron-donating group in the phenyl part of the ppy ligand enhances the emission properties.[8] Ppy ligands with an electron donating group on the phenyl ring in *para* position of the Pt atom leads to Pt(II) complexes with a red-shifted emission and increased emission quantum yield with regards to analogues bearing ppy ligands modified by electron-donating group in *para* position of the pyridyl moiety.[9]

The pyrimidine (1,3-diazine) heterocycle exhibits a stronger electron-deficient character than pyridine due to the presence of the second nitrogen atom.[10] The pyrimidin-2-yl and

pyrimidin-4-yl fragments are therefore stronger electron-withdrawing groups than pyridin-2-yl moiety. 2-Phenylpyrimidine derivatives with electron-donating substituent on the phenyl ring in *para* position generally exhibit fluorescence properties.[11] Whereas many Ir(III) complexes based on N^C 2-phenylpyrimidine ligands are well known in the literature,[12] similar Pt(II) complexes are much less explored.[13]

Recently, Zhao and coworkers have described a 2-(4-*N*,*N*-diphenylaminoyphenyl)pyrimidine Pt(II) complex bearing pyridine and Cl^- as auxiliary ligands.[7a] This complex exhibits strong emission in solid state (Φ_{PL} = 0.45 in PMMA matrix) and promising electroluminescence properties and appears as an efficient emitter for OLEDs. In this contribution, we designed a series of phenylpyrimidine Pt(II) complexes with similar auxiliary ligands (Figure 1). In particular, the nature and the position of substituents along the phenyl ring of the phenylpyrimidine ligand and their influence on photophysical properties have been thoroughly studied.

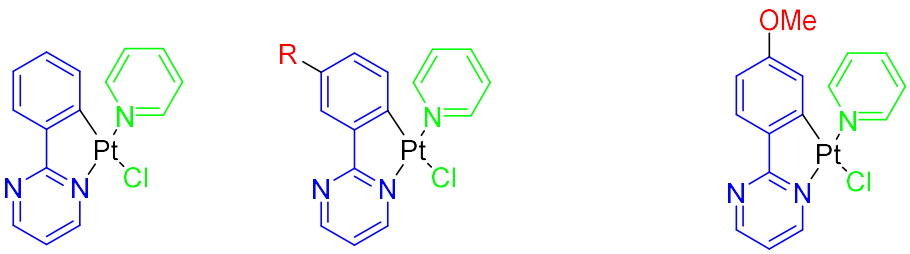

Pt-Pi1

Pt-Pi2: R = CN
Pt-Pi3: R = OMe
Pt-Pi4: R = NPh_2

Pt-Pi5

Figure 1: Structure of studied complexes

Results and discussion

Synthesis

The synthesis of phenylpyrimidine ligands **1-5** and Pt complexes **Pt-Pi** is described in **Scheme 1**. The ligands **1-5** can be easily prepared from commercially available 2-

chloropyrimidine and appropriate phenyl boronic acids via Suzuki-Miyaura cross-coupling reaction.[14] The electron deficient character of pyrimidine allows easier oxidative addition of Pd into carbon-chlorine bond, and therefore, the cross-coupling reaction can be carried out without using a sophisticated and expensive Pd-catalyst.[15] Final Pt-complexes were prepared according to well-established "bridge-splitting" reaction.[7,16] The reaction of $K_2[PtCl_4]$ and the corresponding ligand **1-5** leads to μ-chloro bridged intermediate, which underwent cleavage with pyridine to afford target complexes **Pt-Pi** in moderate-to-good yields.

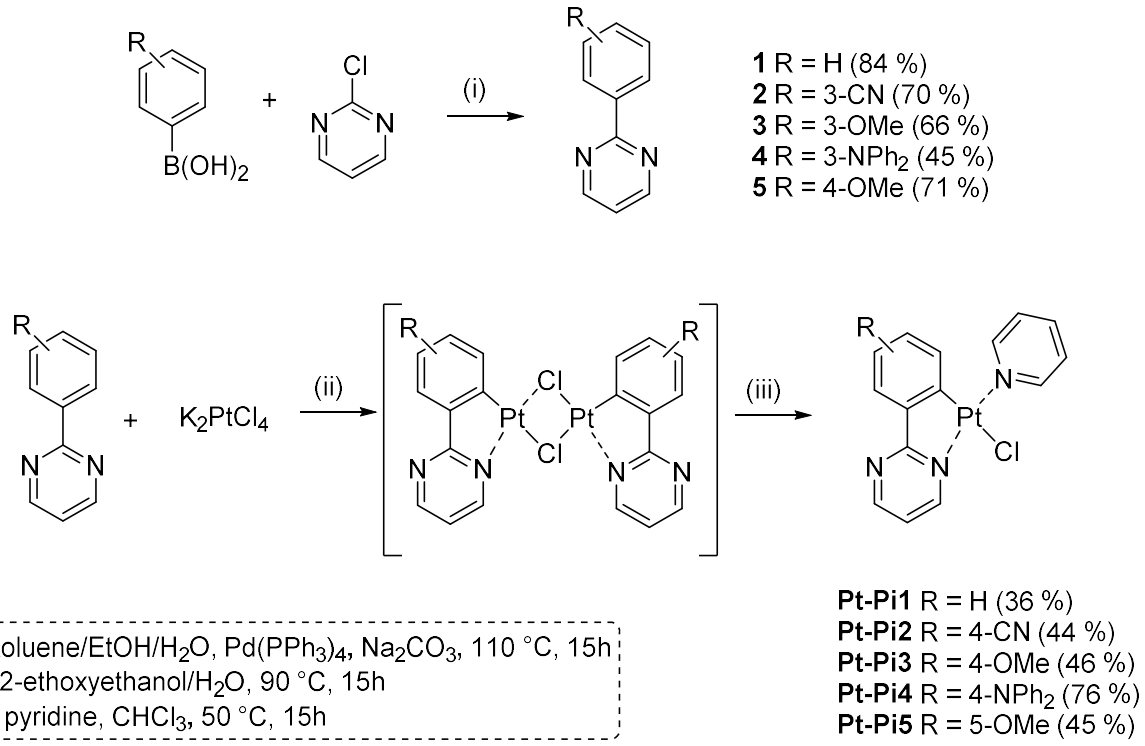

Scheme 1: Synthesis of ligands **1-5** and Pt-complexes **Pt-Pi1-5**. NB: for target complexes, the position of substituent is indicated with regards to the Pt atom.

X-ray-analysis

A single crystal of **Pt-Pi1** was isolated as a yellow prism by slow evaporation of a hexane/ethylacetate (1/1) solution at room temperature. **Pt-Pi1** crystal has been described in orthorhombic symmetry and P*bca* space group. Refinement details and summary of the

structure are given in Table S1. Selected bond distances, bond angles and an ORTEP drawing of the molecule are presented in Table 1 and Figure 2.

The geometry is square-planar with *trans* C,Cl, *trans* N,N chelating positions. The bond lengths C11-Pt1 (1.989(4) Å), Pt1-N22 (2.018(3) Å), Pt1-N1 (2.021(3) Å) are similar to those previously reported for *trans* N,N *tran*s C,Cl platinum complexes.[7,17] The square-planar geometry is slightly distorted with smaller angles between C11-Pt1-N22 (87.13(16)°) and Cl1-Pt1-N1 (87.48(9) °). As previously observed, the torsion angle value between the pyridine ring and the square-plane is 67,66(32)° (C11-Pt1-N1-C6), indicating a possible free rotation of the pyridine ligand around the N1-Pt1 bond in the solution.[7a] This behavior is most likely responsible for low luminescence in solution at room temperature by lowering the radiative decay from T1 or the intersystem cross coupling (S1/T1). On the contrary, this rotation is restricted in the solid state. The packing structure of **Pt-Pi1** (Figure S1) in the solid state shows possible interactions between molecules in inverted positions. The lowest measured distance between the pyrimidine moiety of the square-plane of one molecule and the platinum atom of the parallel monomer is 3.49 Å. This value is close to those observed for electroluminescent cyclometalled platinum complexes that proved to form a stacked dimer by Pt-π interaction (centroid of the nitrogen ring). [18]

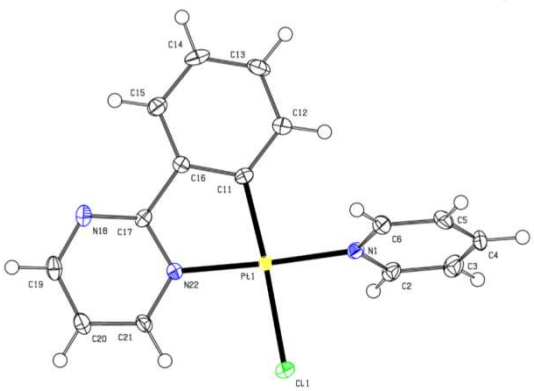

Figure 2: Oak Ridge thermal ellipsoid plot (ORTEP) drawing of complex **Pt-Pi1** (50 % probability level).

.

Table 1 : Selected bond lengths (A), angles and torsion angles (°) for **Pt-Pi1**

Pt1-Cl1	2.4010 (10)
Pt1-N22	2.018 (3)
Pt1-C11	1.989 (4)
Pt1-N1	2.021 (3)
C11-Pt1-N22	81.13 (16)°
C11-Pt1-N1	95.86 (15)°
N22-Pt1-Cl1	95.48 (10)°
N1-Pt1-Cl1	87.48 (9)°
C11-Pt1-N1-C6	67.66(32) °
C11-Pt1-N1-C2	117.15(31) °

Photophysical properties

The photophysical properties of complexes **Pt-Pi1-5** were measured in diluted CH_2Cl_2 solution and the results are reported in Table 2. Various absorption bands are observed below 450 nm (Figure 3a). The most intense band in the 250-300 nm range is attributed to intramolecular ligand π-π* transition. A significant bathochromic shift of this band is observed in the case of diphenylamino complex **Pt-Pi4**. For all complexes, two or three less intense bands/shoulders can be also observed. In an aerated solution, no emission was detected for these compounds (Figure 4) but after bubbling with nitrogen, an emission band centered at 570 and 628 nm with photoluminescence quantum yield of 0.40 and 0.05 was observed for complexes **Pt-Pi3** and **Pt-Pi4** respectively (Figure S25). In both cases a long emission lifetime around 10 μs, characteristic of phosphorescence, emission was observed.

These relatively low quantum yields or none emission of other complexes can be ascribed to possible rotation of the coordinated pyridine ring, which allows non-radiative deexcitation pathway.[7a] In the solid state (powder) all complexes are brightly luminescent and display structured emission profile (Figure 5). This turn-on emission for complexes **Pt-Pi1-2** and **Pt-Pi5** is attributed to restricted rotation of the pyridine ligand in the solid state.[7a] Complexes **Pt-Pi1** and **Pt-Pi5** without any substituent on the phenyl ring in *para* position of the Pt atom, exhibit the most blue-shifted emission maxima (green emission). Complex **Pt-Pi2** with electron-withdrawing cyano group exhibit yellow emission. **Pt-Pi3** and **Pt-Pi4** with electron-donating substituents in conjugative position with respect to the Pt atom are the most red-shifted and the position of the main band follow the strength of the electron-donating group (OMe < NPh_2) and emit orange and red light respectively.

Table 2: UV/Vis and PL data of **Pt-Pi1-5** complexes in CH_2Cl_2 and solid state.

		CH_2Cl_2[a]				Solid State	
		PL				PL	
Compd	UV/vis λ_{max}, nm (ε, $mM^{-1}\cdot cm^{-1}$)	λ_{max}, nm	τ (µs)	Φ_{PL}	Stokes shift cm^{-1}	λ_{max}, nm	τ (µs)
Pt-Pi1	249 (38.8), 286 (13.9)sh, 338 (6.1), 386 (2.0)	–	–	–	–	517, 535, 549	0.51, 2.72
Pt-Pi2	256 (43.4), 270 (36.2), 335 (4.5), 382 (2.1)	–	–	–	–	478, 505, 549, 590sh	0.30, 2.58
Pt-Pi3	251 (44.4), 283 (14.7)sh, 346 (5.5), 414	570	12.9	0.40	6610	591, 630sh	0.47, 2.05

	(2.6)						
Pt-Pi4	285 (27.0), 292 (35.2), 438 (2.3)	628	8.86	0.05	6907	629	0.40, 2.13
Pt-Pi5	264 (24.1), 314 (14.2), 384 (1.8)	–	–	–	–	515, 539, 556	0.34, 1.32

[a] All spectra were recorded at room temperature at $c = 0.9 \times 10^{-5}$ to 1.02×10^{-5} M with deoxygenated solutions prepared by bubbling N_2 through the solutions. [b] Photoluminescence quantum yield (±10%) determined relative to 9,10-bisphenylethynylanthracene in cyclohexane ($\Phi_{PL} = 1.00$).[19]

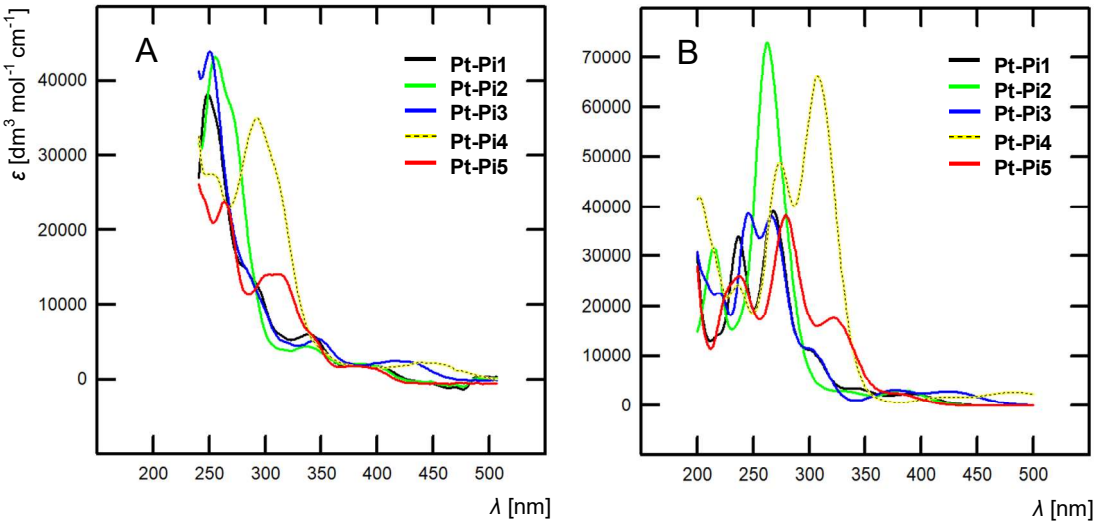

Figure 3: (A) Absorption spectra of compounds **Pt-Pi1–5** (c = 0.9 – 1.5×10^{-5} mol.l^{-1}) in CH_2Cl_2. **(B)** TD-DFT-simulated spectra.

10.1002/ejic.202100155

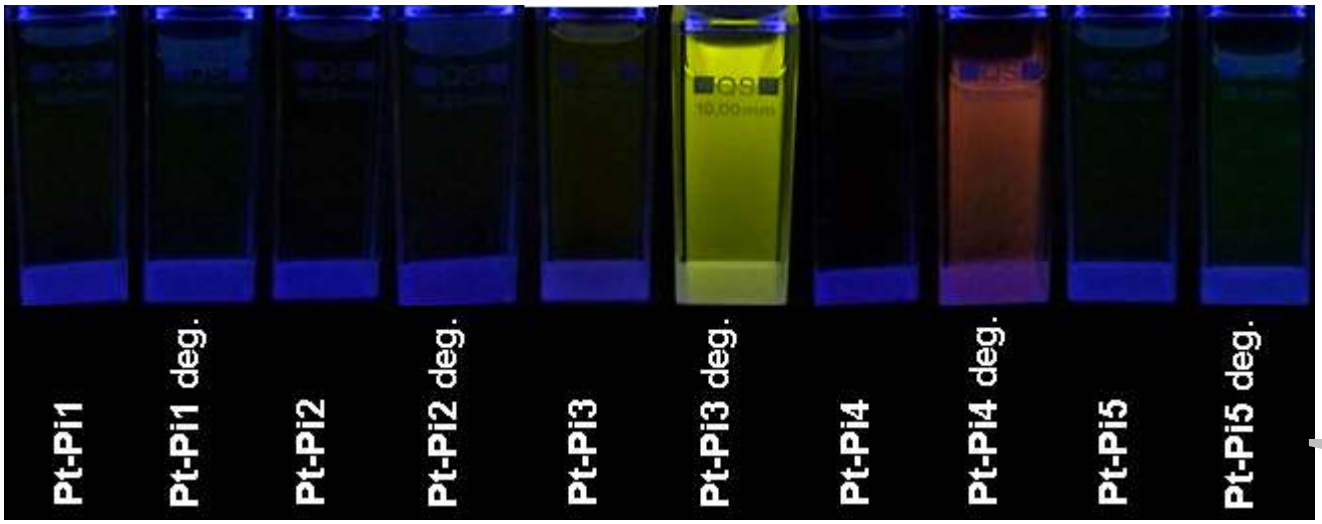

Figure 4: Picture of CH_2Cl_2 solution of **Pt-Pi1–5** (oxygenated/degassed) taken under UV (λ = 240 nm).

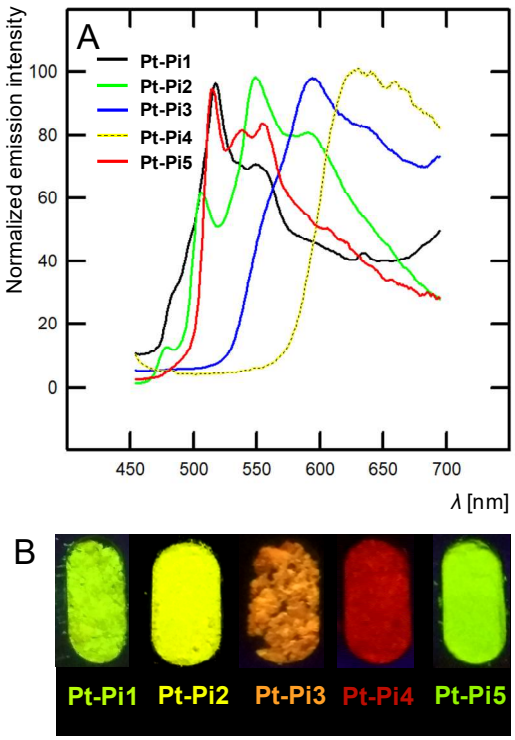

Figure 5: Normalized emission spectra of solid state compounds **Pt-Pi1–5** and picture taken under UV (λ = 240 nm)

Computational investigation

Density functional theory (DFT) calculations at the PBE0/LANL2DZ level of theory were performed to optimize the geometries of complexes **Pt-Pi1–5**. Solvent ($CHCl_3$) effect corrections were included (see Computational Details). The five optimized structures are shown in Figure 6. Selected computed data are provided in Table 3. The optimized geometry of **Pt-Pi1** is very close to its X-ray structure, with slightly longer metal-ligands bonds as usually found for DFT-optimized structures. Complexes **Pt-Pi1–5** exhibit very similar optimized geometries with analogous metrical data. The calculated angles between the pyridine ligand and the Pt coordination plane lie within a narrow range of 65-67°, which is very close to the experimental angle found for **Pt-Pi1 (**67.7°, Table 2). The shortest calculated inter-molecular H…H contact lies within the range of 2.7-2.8 Å. This observation suggests that the pyridine rotational position is a trade-off between conjugation (which favors planarity) and H…H steric repulsion (which prefers perpendiculatity). As a matter of fact, forcing the two planes to be perpendicular destabilizes **Pt-Pi1**, but only by 0.01 eV. It is therefore very likely that in solution, the pyridine ligand affords a vibrational motion of several tenths of degrees.

10.1002/ejic.202100155

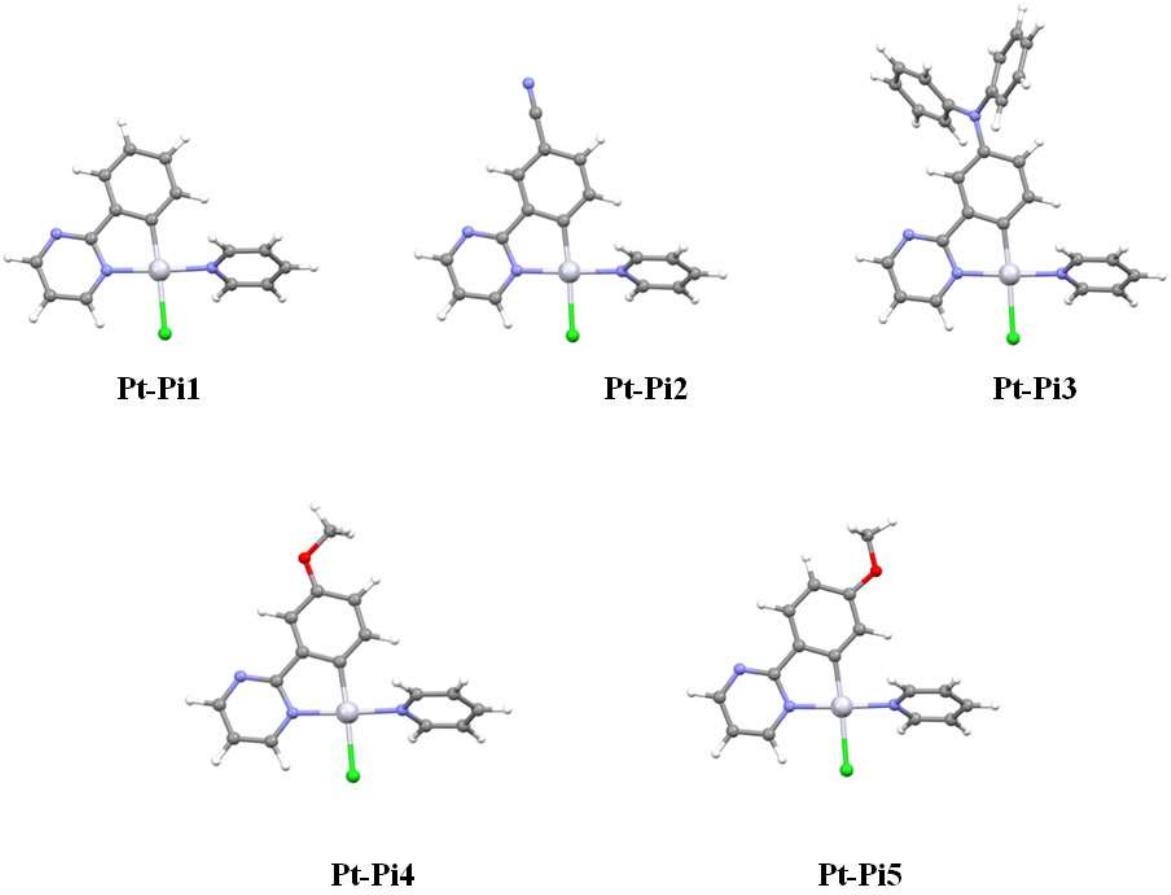

Figure 6: DFT-optimized geometries of complexes **Pt-Pi1–5**.

Compound		**Pt-Pi1**	**Pt-Pi2** CN	**Pt-Pi3** OMe	**Pt-Pi4** NPh_2	**Pt-Pi5** OMe
HOMO-LUMO gap (eV)		4.15	4.19	3.80	3.28	4.23
Pt-Cl (Å) [Wiberg bond indice]		2.454 [0.301]	2.440 [0.312]	2.454 [0.301]	2.453 [0.303]	2.454 [0.302]
Pt-N(py) (Å) [Wiberg bond indice]		2.020 [0.396]	2.020 [0.399]	2.019 [0.398]	2.019 [0.398]	2.021 [0.395]
Pt-N(ppy) (Å) [Wiberg bond indice]		2.016 [0.411]	2.019 [0.408]	2.017 [0.411]	2.017 [0.410]	2.016 [0.412]
Pt-C(ppy) (Å) [Wiberg bond indice]		1.978 [0.689]	1.971 [0.696]	1.981 [0.679]	1.978 [0.687]	1.977 [0.686]
Py/Pt(ppy) torsion angle (°)		66	67	65	65	65
NAO charges	Pt	0.63	0.65	0.63	0.64	0.63
	Cl	-0.69	-0.68	-0.69	-0.69	-0.69
	N(py)	-0.52	-0.52	-0.52	-0.52	-0.52
	N(ppy)	-0.54	-0.54	-0.54	-0.54	-0.55
	C(ppy)	-0.19	-0.17	-0.22	-0.20	-0.17

Table 3: Relevant computed data for complexes **Pt-Pi1–5**.

The Natural Atomic Orbital charges and the metal-ligand Wiberg bond indices of the five complexes are also very close. The largest atomic charge variation concerns the carbon bonded to the metal, which obeys the electronic effects of the substituent appended on the phenyl ring. These are particularly pronounced from the position 4 of the phenyl (Scheme 1), from which the π-donor substituents OMe and NPh_2 tend to favor a more negative polarization of the C-atom. A slightly stronger Pt-Cl bond induced by the acceptor CN substituent can be noticed for **Pt-Pi2**. Anyway, these effects on the metal coordination sphere are small. On the contrary, the HOMO-LUMO gaps are affected more significantly, especially for the complexes bearing a π-donor substituent at the position 4 of the phenyl. The calculated gaps are smaller, which is in agreement to experimentally observed variations of the optical

properties (see above). The Kohn-Sham diagrams of the five complexes (Figure S22) and the plots of their frontier orbitals (Figure S23) provide more insight into their electronic structures. According to the electronic effect of the substituent appended on the phenyl ring, they can be divided into three groups. The first one possesses π-donor in a conjugative position with respect to the metal, **Pt-Pi3** and **Pt-Pi4** exhibit a destabilized HOMO having a substantial phenylpyrimidine character to which the substituent's lone pair contributes. The second group is made of **Pt-Pi1** and **Pt-Pi5** (no substituent or mesomeric effect), with the HOMO having less, but still significant, contribution from the phenylpyrimidine ligand. **Pt-Pi2** constitutes the third group, in which the highest occupied levels are stabilized by the electron-withdrawing effect of the substituent. The vacant levels are also slightly stabilized, so that its HOMO-LUMO gap is not the largest one within the series. The lowest vacant orbitals of **Pt-Pi1–5** possess π*(ligand) character, whereas their LUMO is of π*(phenylpyrimidine) nature.

The TD-DFT-simulated UV-vis spectra of compounds **Pt-Pi1–5** are shown on Figure 3b. They are in a rather good agreement with their experimental counterparts (Figure 3a). The computed transitions responsible for the major bands on the simulated spectra are reported in Table 4. The lowest-energy band corresponds to the HOMO→LUMO transition. Figure S23 implies that it has a mixed electron-transfer character, with a dominant intra-phenylpyrimidine character. The other bands do not show important long-range transfer neither dominant metal participation.

The simulated phosphorescence spectra of the two compounds that are emissive in solution, namely **Pt-Pi3** and **Pt-Pi4,** were calculated by using the Adiabatic Hessian (AH) method developed by Barone and coworkers,[20] the efficiency of which was recently proven when applied to platinum complexes.[21] The corresponding simulated spectra are shown in Figure S24. Their intensity maxima are reported in Table 4, together with the corresponding

10.1002/ejic.202100155

experimental λ_{max} values. The agreement is quite good, thus allowing to identify the transitions as originating from an excited $(HOMO)^1(LUMO)^1$ triplet state.

Table 4: Absorption: The major computed transitions (λ_{calc}) associated with their experimental UV-vis λ_{max} counterparts. Emission: Computed and experimental phosphorescence λ_{max}.

Compd.	Absorption: Experimental UV/vis λ_{max}, nm (ε, $mM^{-1}\cdot cm^{-1}$)	Absorption: Computed major contribution to the band in Figure 2b λ_{calc} nm	Absorption: Nature of the transition	Emission: Experimental λ_{max}, nm	Emission: Computed λ_{max}, nm (see Fig. S24)
Pt-Pi1	386 (2.0)	392 (0.03)	ILCT[a] + MLCT[b] +LLCT[c]	-	
	338 (6.1)	303 (0.11)	ILCT[a] + MLCT[b]		
	286 (13.9)sh				
	249 (38.8)	277 (0.10)	ILCT[a] + LLCT[d]		
Pt-Pi2	382 (2.1)	385 (0.04)	ILCT[a] + MLCT[b] +LLCT[c]	-	
	335 (4.5)	304 (0.11)	ILCT[a] + MLCT[b]		
	270 (36.2)				
	256 (43.4)	282 (0.17)	ILCT[a] + LLCT[d]		
Pt-Pi3	414 (2.6)	428 (0.04)	ILCT[a] + MLCT[b] +LLCT[c]	570	578
	346 (5.5)	304 (0.12)	ILCT[a] + MLCT[b]		**532**
	283 (14.7)sh				
	251 (44.4)	277 (0.13)	ILCT[a] + LLCT[d]		
Pt-Pi4	438 (2.3)	485 (0.04)	ILCT[a] + LLCT[c]	628	**662**
	292 (35.2)	316 (0.19)	LLCT[d] + MLCT[b]		614
	285 (27.0)	275 (0.26)	ILCT[a] + LLCT[d]		
Pt-Pi5	384 (1.8)	380 (0.03)	ILCT[a] + MLCT[b] +LLCT[c]	-	
	314 (14.2)	299 (0.12)	LLCT[d] + MLCT[b]		
	264 (24.1)	280 (0.40)	ILCT[a] + LLCT[d]		

[a] $\pi\rightarrow\pi^*$ phenylpyrimidine . [b]Pt$\rightarrow$phenylpyrimidine. [c] Cl$\rightarrow$phenylpyrimidine.
[d] phenylpyrimidine$\rightarrow$pyridine.

Conclusion

Five Pt(II) complexes with varied electron behavior of the appended 2-phenylpyridimidine ligands were designed and prepared. It has been demonstrated that proper substitution of the 2-phenylpyrimidine significantly influences optical properties of developed Pt(II) complexes. A conjugative interconnection of the electron-donor and the metal center significantly increases the emission quantum yield in the solution and red-shifts emission in the solid state. Strong emission of these complexes in the solid state makes them promising candidates for incorporation in OLED devices. Further modification of the auxiliary ligands to tune and optimize the emission properties are currently ongoing in our laboratories.

Experimental part

General Conditions. Reagents and solvents were reagent-grade and were purchased from Sigma Aldrich or TCI Europe and used as received. NMR spectra were acquired at room temperature at 300/75 MHz with a Bruker AVANCE III. Chemical shifts are given in parts per million relative to TMS (^{1}H, 0.0 ppm) and $CDCl_3$ (^{13}C, 77.0 ppm). Acidic impurities in $CDCl_3$ were removed by treatment with anhydrous K_2CO_3. High resolution MALDI MS spectra were measured on a MALDI mass spectrometer equipped with nitrogen UV laser (337 nm, 60 Hz) and quadrupole analyser (positive-ion mode over a normal mass range (*m/z* 50-2000) with resolution 100 000 at *m/z* = 400). *Trans*-2-[3-(4-*tert*-butylphenyl)-2-methyl-2-propenylidene]malononitrile (DCTB) was used as a matrix. Mass spectra were averaged over the whole MS record for all measured samples. The absorption spectra of the samples in solutions and films were detected with a Jasco V-650 while the emission spectra were detected by a Horiba Fluoromax spectrophotometer respectively. UV-vis and photoluminescence spectra were recorded using standard 1 cm quartz cells. Compounds were excited at their absorption maxima (band with the lowest energy) to record the emission spectra. The Φ_F values were calculated using a well-known procedure with 9,10-diphenylethynylanthracene in cyclohexane as standard (Φ_F = 1).[19] Stokes shifts were calculated by considering the lowest energetic absorption band.

X-Ray Structural Analysis Single-crystal X-ray-diffraction data were obtained from a D8 VENTURE Bruker AXS diffractometer equipped with a (CMOS) PHOTON 100 detector, using Mo-Kα radiation (λ = 0.71073 Å, multilayer monochromator) at T = 150 K. Crystal structure was solved by dual-space algorithm using the SHELXT program,[22] and then refined with full-matrix least-squares methods based on F^2 (SHELXL program).[23] All non-hydrogen atoms were refined with anisotropic atomic displacement parameters. H atoms were finally

included in their calculated positions and treated as riding on their parent atom with constrained thermal parameters. Drawing was produced using ORTEP-3. CCDC-2039829 (**Pt-Pi1**) contains supplementary crystallographic data. These data can be obtained free of charge from the Cambridge Crystallographic Data Centre via www.ccdc.cam.ac.uk/data_request/cif.

Computational details. DFT and TD-DFT calculations were carried out using the Gaussian16 package,[24] employing the PBE0 functional,[25] together with the LanL2DZ basis set.[26] Solvent (chloroform) effects were included through the PCM approximation.[27] The optimized geometries were fully characterized as true minima by analytical frequency calculations (no imaginary values). The composition of the Kohn-Sham orbitals was calculated using the AOMix program.[28] The geometries obtained from DFT calculations were used to perform natural atomic charge analysis with the NBO 6.0 program.[29] Only singlet-singlet transitions were taken into account in the TD-DFT calculations. Only the transitions with non-negligible oscillator strengths are discussed in the paper. The graphical GaussView interface[30] was used for simulating UV-vis spectra. The phosphorescence emission spectra were computed within the Franck-Condon principle by using the Adiabatic Hessian method[31] which takes into account vibrational mode mixing and a proper description of both optimized ground and excited (triplet) states potential energy surfaces. A class-based pre screening[32] was applyied in order to limit the number of terms involved in the vibronic calculation with the following settings: C_1max = 70, C_2max = 70, N_1max = 100 × 10^8. The GaussView interface[30] was used for their simulation (Figure S23).

***General procedure for the synthesis of ligands*:** 2-Chloropyrimidine (1 equiv) and corresponding boronic acid (1.2 equiv) were dissolved in a mixture of toluene/EtOH (20:3, 23mL), and nitrogen was bubbled through the solution for 10 min. $Pd(PPh_3)_4$ (5 %) and 20% aqueous Na_2CO_3 were added, and then the reaction was stirred at 110 °C for 15h. The reaction

mixture was cooled to room temperature and diluted with CH_2Cl_2/aqueous NH_4Cl (1:1, 100 mL). Organic layer was separated, and the aqueous one was extracted with CH_2Cl_2 (2 × 50 mL). The combined organic extracts were dried over anhydrous $MgSO_4$ and solvent was evaporated under reduced pressure. The solid residue was purified by column chromatography (SiO_2; indicated solvents).

***General procedure for the synthesis of Pt^{II} complexes*:** K_2PtCl_4 (1 equiv) and ligand **A** (1.2 equiv) were dissolved in a mixture of EGEE/H_2O (3:1, 20 mL). The mixture was bubbled with nitrogen for 10 min and then stirred at 90 °C for 15h. The solution was cooled to room temperature and diluted with H_2O, precipitate was filtrated off, and dried under vacuum. μ-Chloro-bridged intermediate was dissolved in $CHCl_3$ and pyridine was added (2.5 equiv). The mixture was stirred at 50 °C for 15h. The reaction mixture was cooled to room temperature and diluted with CH_2Cl_2/aqueous NH_4Cl (1:1, 100 mL). The organic layer was separated, and the aqueous one was extracted with CH_2Cl_2 (2 × 50 mL). The combined organic extracts were dried over anhydrous $MgSO_4$ and the solvents were evaporated under reduced pressure. The solid residue was purified by column chromatography (SiO_2; 1:1, EtOAc/CH_2Cl_2).

2-Phenylpyrimidine (**1**): Synthesized from 2-chloropyrimidine (458 mg, 4 mmol) and phenylboronic acid (586 mg, 4.8 mmol) following the general procedure for the synthesis of ligands and purified by column chromatography (8:2, petroleum ether/EtOAc) Yield 524 mg (84 %); pale orange solid. R_f = 0.5 (8:2, petroleum ether/EtOAc). ^{1}H NMR (300 MHz, $CDCl_3$) δ = 8.81 (d, $^3J_{H,H}$ = 5 Hz, 2H), 8.46–8.42 (m, 2H), 7.52–7.47 (m, 3H), 7.19 (t, $^3J_{H,H}$ = 5 Hz, 1H) ppm. The spectroscopic data were consistent with those reported in the literature.[33]

2-(3-Cyanophenyl)pyrimidine (2): Synthesized from 2-chloropyrimidine (458 mg, 4 mmol) and 3-cyanophenylboronic acid (706 mg, 4.8 mmol) following the general procedure for the synthesis of ligands and purified by column chromatography (7:3, petroleum ether/EtOAc) Yield 508 mg (70 %); white solid. R_f = 0.5 (7:3, petroleum ether/EtOAc). ^{1}H NMR (300

MHz, $CDCl_3$) δ = 8.84 (d, $^3J_{H,H}$ = 5 Hz, 2H), 8.79–8.78 (m, 1H)m 8.71–8.68 (m, 1H), 7.78–7.75 (m, 1H), 7.63–7.58 (m, 1H), 7.28 (t, $^3J_{H,H}$ = 5 Hz, 1H) ppm. ^{13}C NMR (75 MHz, $CDCl_3$) δ = 162.80, 157.60, 138.91, 133.99, 132.36, 132.12, 129.57, 120.14, 118.80, 113.09 ppm. HR-MALDI-MS (DCTB) *m/z* calcd for $C_{11}H_8N_3$ [M+H$^+$] 182.0713, found 182.0713. The spectroscopic data were consistent with those reported in the literature.[34]

2-(3-Methoxyphenyl)pyrimidine (3): Synthesized from 2-chloropyrimidine (606 mg, 5.29 mmol) and 3-methoxyphenylboronic acid (965 mg, 6.35 mmol) following the general procedure for the synthesis of ligands and purified by column chromatography (CH_2Cl_2) Yield 651 mg (66 %); pale orange solid. R_f = 0.2 (CH_2Cl_2). ^{1}H NMR (300 MHz, $CDCl_3$) δ = 8.81 (d, $^3J_{H,H}$ = 5 Hz, 2H), 8.07–8.00 (m, 2H), 7.43–7.38 (m, 1H), 7.19 (t, $^3J_{H,H}$ = 5 Hz, 1H), 7.07–7.03 (m, 1H), 3.91 (s, 3H) ppm. HR-MALDI-MS (DCTB) *m/z* calcd for $C_{11}H_{11}N_2O$ [M+H$^+$] 187.0866, found 187.0866. The spectroscopic data were consistent with those reported in the literature.[34]

2-(3-N,N-Diphenylaminophenyl)pyrimidine (4): Synthesized from 2-chloropyrimidine (96 mg, 0.83 mmol) and 3-*N,N*-diphenylaminophenylboronic acid (289 mg, 1 mmol) following the general procedure for the synthesis of ligands and purified by column chromatography (CH_2Cl_2) Yield 122 mg (45 %); white solid. R_f = 0.6 (CH_2Cl_2). ^{1}H NMR (300 MHz, $CDCl_3$) δ = 8.75–8.73 (m, 2H), 8.22–8.21 (m, 1H), 8.10–8.07 (m, 1H), 7.40–7.35 (m, 1H), 7.28–7.19 (m, 4H), 7.17–6.99 (m, 8H) ppm. ^{13}C NMR (75 MHz, $CDCl_3$) δ = 164.70, 157.31, 148.50, 148.00, 139.14, 129.67, 129.40, 126.98, 124.32, 124.17, 122.86, 119.22 ppm. HR-MALDI-MS (DCTB) *m/z* calcd for $C_{22}H_{17}N_3$ [M$^+$] 323.1417, found 323.1405.

2-(4-Methoxyphenyl)pyrimidine (5): Synthesized from 2-chloropyrimidine (615 mg, 5.36 mmol) and 4-methoxyphenylboronic acid (978 mg, 6.44 mmol) following the general procedure for the synthesis of ligands and purified by column chromatography (CH_2Cl_2)

Yield 706 mg (71 %); pale yellow solid. R_f = 0.2 (CH_2Cl_2). ^{1}H NMR (300 MHz, $CDCl_3$) δ = 8.75 (d, $^3J_{H,H}$ = 5 Hz, 2H), 8.41–8.37 (m, 2H), 7.11 (t, $^3J_{H,H}$ = 5 Hz, 1H), 7.03–6.98 (m, 2H), 3.88 (s, 3H) ppm. HR-MALDI-MS (DCTB) *m/z* calcd for $C_{11}H_{11}N_2O$ [M+H$^+$] 187.0866, found 187.0866. The spectroscopic data were consistent with those reported in the literature.[35]

(**Pt-Pi1**): Synthesized from K_2PtCl_4 (100 mg, 0.24 mmol) and **1** (46 mg, 0.29 mmol) following the general procedure for the synthesis of Pt^{II} complexes. Yield 40 mg (36 %) yellow solid. R_f = 0.5 (1:1, EtOAc/CH_2Cl_2). ^{1}H NMR (300 MHz, $CDCl_3$) δ = 9.87–9.73 (m, $^3J_{H,Pt}$ = 38 Hz, 1H), 9.08–8.91 (m, $^3J_{H,Pt}$ = 47 Hz, 2H), 8.79–8.77 (m, 1H), 7.94–7.85 (m, 2H), 7.47–7.42 (m, 2H), 7.17–7.05 (m, 3H), 6.47–6.28 (m, $^3J_{H,Pt}$ = 49 Hz, 1H) ppm. ^{13}C NMR (75 MHz, $CDCl_3$) δ = 175.83, 158.56, 157.56 (m, $^2J_{C,Pt}$ = 8 Hz), 154.18 (m, $^2J_{C,Pt}$ = 6 Hz), 141.66, 141.09, 138.13 (m, $^2J_{C,Pt}$ = 6 Hz), 132.46 (m, $^3J_{C,Pt}$ = 29 Hz), 130.37 (m, $^3J_{C,Pt}$ = 23 Hz), 127.79 (m, $^3J_{C,Pt}$ = 23 Hz), 126.22 (m, $^3J_{C,Pt}$ = 26 Hz), 124.23, 117.65 (m, $^4J_{C,Pt}$ = 14 Hz), ppm. HR-MALDI-MS (DCTB) *m/z* calcd for $C_{15}H_{12}ClN_3Pt$ [M$^+$] 464.0362, found 464.0365.

(**Pt-Pi2**): Synthesized from K_2PtCl_4 (200 mg, 0.48 mmol) and **2** (105 mg, 0.58 mmol) following the general procedure for the synthesis of Pt^{II} complexes. Yield 40 mg (36 %) yellowish solid. R_f = 0.6 (1:1, EtOAc/CH_2Cl_2). ^{1}H NMR (300 MHz, $CDCl_3$) δ = 9.93–9.79 (m, $^3J_{H,Pt}$ = 38 Hz, 1H), 9.01–8.86 (m, 3H), 8.22–8.03 (m, 1H), 8.00–7.91 (m, 1H), 7.53–7.49 (m, 2H), 7.31–7.24 (m, 2H), 6.60–6.42 (m, $^3J_{H,Pt}$ = 49 Hz, 1H) ppm. (75 MHz, $CDCl_3$) δ = 158.96, 157.84, 153.99 (m, $^2J_{C,Pt}$ = 6 Hz), 148.15, 138.67, 134.89 (m, $^3J_{C,Pt}$ = 29 Hz), 131.14, 130.69, 129.88, 126.58 (m, $^3J_{C,Pt}$ = 25 Hz), 119.63, 118.72 (m, $^4J_{C,Pt}$ = 14 Hz), 107.38 ppm (One quaternary carbon is not observed due to the low solubility of this complex). HR-MALDI-MS (DCTB) *m/z* calcd for $C_{16}H_{11}ClN_4Pt$ [M$^+$] 489.0315, found 489.0317.

(**Pt-Pi3**): Synthesized from K_2PtCl_4 (100 mg, 0.24 mmol) and **3** (54 mg, 0.29 mmol) following the general procedure for the synthesis of Pt^{II} complexes. Yield 55 mg (46 %) orange solid. R_f = 0.6 (1:1, EtOAc/CH_2Cl_2). ^{1}H NMR (300 MHz, $CDCl_3$) δ = 9.85–9.70 (m, $^3J_{H,Pt}$ = 34 Hz, 1H), 9.07–8.91 (m, $^3J_{H,Pt}$ = 45 Hz, 2H), 8.77–8.74 (m, 1H), 7.93–7.87 (m, 1H), 7.46–7.41 (m, 3H), 7.10–7.07 (m, 1H), 6.76–6.72 (m, 1H), 6.36–6.17 (m, $^3J_{H,Pt}$ = 48 Hz, 1H), 3.62 (s, 3H) ppm. ^{13}C NMR (75 MHz, $CDCl_3$) δ = 175.63, 158.33, 157.63 (m, $^2J_{C,Pt}$ = 10 Hz), 157.14, 154.17 (m, $^2J_{C,Pt}$ = 6 Hz), 142.08, 138.04 (m, $^2J_{C,Pt}$ = 6 Hz), 131.96, 131.04 (m, $^3J_{C,Pt}$ = 28 Hz), 126.17 (m, $^3J_{C,Pt}$ = 26 Hz), 120.07 (m, $^3J_{C,Pt}$ = 31 Hz), 117.69 (m, $^4J_{C,Pt}$ = 17 Hz), 111.38 (m, $^3J_{C,Pt}$ = 25 Hz), 55.55 ppm. HR-MALDI-MS (DCTB) *m/z* calcd for $C_{16}H_{14}ClN_3OPt$ [M^+] 494.0468, found 494.0472.

(**Pt-Pi4**): Synthesized from K_2PtCl_4 (100 mg, 0.24 mmol) and **4** (94 mg, 0.29 mmol) following the general procedure for the synthesis of Pt^{II} complexes. Yield 115 mg (76 %) orange solid. R_f = 0.8 (1:1, EtOAc/CH_2Cl_2). ^{1}H NMR (300 MHz, $CDCl_3$) δ = 9.86–9.74 (m, $^3J_{H,Pt}$ = 34 Hz, 1H), 9.07–8.92 (m, $^3J_{H,Pt}$ = 44 Hz, 2H), 8.70–8.68 (m, 1H), 7.91–7.86 (m, 1H), 7.70–7.69 (m, 1H), 7.45–7.41 (m, 2H), 7.23–7.18 (m, 4H), 7.10–7.06 (m, 5H), 7.98–6.88 (m, 3H), 6.40–6.22 (m, $^3J_{H,Pt}$ = 48 Hz, 1H) ppm. ^{13}C NMR (75 MHz, $CDCl_3$) δ = 175.26, 158.43, 157.64 (m, $^2J_{C,Pt}$ = 10 Hz), 154.11, 147.84, 144.50, 142.58, 138.09, 135.36, 131.19 (m, $^3J_{C,Pt}$ = 28 Hz), 129.77 (m, $^3J_{C,Pt}$ = 31 Hz), 129.28, 126.16 (m, $^3J_{C,Pt}$ = 26 Hz), 124.49 (m, $^3J_{C,Pt}$ = 24 Hz), 123.54, 122.36, 117.73 (m, $^4J_{C,Pt}$ = 13 Hz), ppm. HR-MALDI-MS (DCTB) *m/z* calcd for $C_{27}H_{22}ClN_4Pt$ [M^+] 632.1175, found 632.1094.

(**Pt-Pi5**): Synthesized from K_2PtCl_4 (100 mg, 0.24 mmol) and **5** (54 mg, 0.29 mmol) following the general procedure for the synthesis of Pt^{II} complexes. Yield 54 mg (45 %) yellow solid. R_f = 0.4 (1:1, EtOAc/CH_2Cl_2). ^{1}H NMR (300 MHz, $CDCl_3$) δ = 9.78–9.64 (m, $^3J_{H,Pt}$ = 39 Hz, 1H), 9.08–8.89 (m, $^3J_{H,Pt}$ = 46 Hz, 2H), 8.72–8.69 (m, 1H), 7.93–7.87 (m, 1H), 7.84–7.82 (m, 1H), 7.47–7.42 (m, 2H), 7.02–6.99 (m, 1H), 6.71–6.68 (m, 1H), 5.95–5.76 (m,

$^{3}J_{H,Pt}$ = 56 Hz, 1H), 3.68 (s, 3H) ppm. ^{13}C NMR (75 MHz, $CDCl_3$) δ = 175.20, 162.79, 158.57, 157.50 (m, $^{2}J_{C,Pt}$ = 11 Hz), 154.17 (m, $^{2}J_{C,Pt}$ = 6 Hz), 142.79, 138.13 (m, $^{2}J_{C,Pt}$ = 6 Hz), 134.41, 129.56 (m, $^{3}J_{C,Pt}$ = 27 Hz), 126.17 (m, $^{3}J_{C,Pt}$ = 26 Hz), 116.50 (m, $^{3}J_{C,Pt}$ = 24 Hz), 116.43 (m, $^{4}J_{C,Pt}$ = 19 Hz), 108.86, 55.17 ppm. HR-MALDI-MS (DCTB) *m/z* calcd for $C_{16}H_{14}ClN_3OPt$ [M^+] 494.0468, found 494.0476.

Acknowledgements

M. F. acknowledges the Région Bretagne, France, for her Ph. D. funding (HOLED project)

[1] a) L. Bischoff, C. Baudequin, C. Hoarau, E. P. Urriolabeitia, *Adv. Organomet. Chem.*, **2018**, *69*, 73-134; b) V. W.-W. Yam, V. K.-M. Au, S. Y.-L. Leung, *Chem. Rev.*, **2015**, *115*, 7589-7728; c) X. Zhang, Y. Hou, X. Xiao, X. Chen, M. Hu, X. Geng, Z. Wang, J. Zhao, *Coord Chem. Rev.*, **2020**, *417*, 213371; d) P.-Y. Ho, C.-L. Ho, W.-Y. Wong, *Coord. Chem. Rev.*, **2020**, *413*, 213267; e) C. Cébrián, M. Mauro, *Beilstein J. Org. Chem.*, **2018**, *14*, 1459-1481; f) X. Cui, J. Zhao, Z. Mohmood, C. Zhang, *Chem. Rec.*, **2016**, *16*, 173-188.

[2] a) M. Y. Wong, E. Zysman-Colman, *Adv. Mater.* **2017**, *29*, 1605444; b) C. Fang, C. Yang, *Chem. Soc. Rev.*, **2014**, *43*, 6439-6469.

[3] a) X. Zeng, M. Tavasli, I. F. Perepichka, A. S. Batsanov, M. R. Bryce, C.-J. Chiang, C. Rothe, A. P. Monkman, *Chem. Eur. J.*, **2008**, *14*, 933-943; b) T. T. Dang, M. Bonneau, J. A. Williams, H. Le Bozec, H. Doucet, V. Guerchais, *Eur. J. Inorg. Chem.*, **2015**, 2956-5964; c) M. Lepeltier, H. Le Bozec, V. Guerchais, T. K.-M. Lee, K. K.-W. Lo, *Organometallics*, **2005**, *24*, 6069-6072 ; d) Y. Zhang, X. Chen, D. Song, D. Zhong, X. Yang, Y. Sun, B. Liu, G. Zhou, Z. Wu, *Inorg. Chem. Frontiers*, **2020**, *7*, 1651-1666.

[4] a) J. Kalinowski, V. Fattori, M. Cocchi, J. A. G. Williams *Coord. Chem. Rev.*, **2011**, *255*, 2401-2425; b) W.-Y. Wong, C.-L. Ho, *J. Mater. Chem.*, **2009**, *19*, 4457-4482; c) F.

Niedermair, O. Kwon, K. Zojer, S. Kappaun, G. Trimmel, K. Mereiter. C. Slugovc, *Dalton Trans.*, **2008**, 4006-4014; d) B. L. Yin, F. Niemeyer, J. A. G. Williams, J. Jiang, A. Boucekkine, L. Toupet, H. Le Bozec, V. Guerchais, *Inorg. Chem.*, **2006**, *45*, 8584-8596; e) A. Valore, A. Colombo, C. Dragonetti, S. Righetto, D. Roberto, R. Ugo, F. De Angelis, S. Fatacci, *Chem. Commun.*, **2010**, *46*, 2414-2416; f) M. Ghdini, T. Pugliese, M. La Deda, N. Godbert, I. Aiello, M. Amati, S. Belviso, F. Lelj, G. Accorsi, F. Bariegelletti, *Dalton Trans.*, **2008**, *32*, 4303-4318.

[5] J. Brooks, Y. Babayan, S. Lamansky, P. I. Djurivich, I. Tsyba, R. Bau, M. E. Thompson, *Inorg. Chem.*, **2002**, *41*, 3055-3066.

[6] a) G. Zhou, Q. Wng, X. Wang, C.-L. Ho, W.-Y. Wong, D. Ma, L. Wang, Z. Lin*, J. Mater. Chem.*, **2010**, *20*, 7472-7484; b) S. Akagi, S. Fujii, N. Kitamura, *Dalton Trans.*, **2020**, *49*, 6363-6367; c) Y. Yan, Z. Yu, C. Liu, X. Jin, *Dyes Pigm.*, **2020**, *173*, 107949.

[7] a) J. Zhao, F. Dang, Z. Feng, B. Liu, X. Yang, Y. Wu, G. Zhou, Z. Wu, W.-Y. Wong, *Chem. Commun.*, **2017**, *53*, 7581-7584; b) J. Zhao, Z. Feng, D. Zhog, X. Yang, Y. Wu, G. Zhou, Z. Wu, *Chem. Mater.*, **2018**, *30*, 929-946.

[8] A. Santoro, A. C. Whitwood, J. A. G. Williams, V. N. Kozhevnikov, D. W. Bruce, *Chem. Mater.*, **2009**, *21*, 3871-3882.

[9] C. Yang, X. Zhang, H. You, L. Zhu, L. Chen, L. Zhu, Y. Tao, D. Ma, Z. Shuuai, J. Qin, *Adv. Funct. Mater.*, **2007**, 17, 651-661.

[10] a) R. Komatsu, H. Sasabe, J. Kido, *J. Photonics Ener.*, **2018**, *8*, 032108; b) K.-C.; Pan, S.-W. Li, Y.-J. Shiu, W.-L. Tsai, M. Jiao, W.-K. Lee, C.-C. Chung, T. Chatterjee, Y.-S. Li, K.-T. Wong, H.-C. Hu, C.-C. Chen, M.-T. Lee, *Adv. Funct. Mater.*, **2016**, *26*, 7560-7571.

[11] a) S. Achelle, J. Rodríguez-López, F. Robin-le Guen, *ChemistrySelect*, **2018**, *3*, 1852-1886; b) S. Achelle, J. Rodríguez-López, M. Larbani, R. Plaza-Pedroche, F. Robin-le Guen,

Molecules, **2019**, *24*, 1742; c) C. Denneval, S. Achelle, C. Baudequin, F. Robin-le Guen, *Dyes Pigm.*, **2014**, *110*, 49-55.

[12] a) H. Ma, D. Liu, J. Li, Y. Mei, D. Li, Y. Ding, W. Wei, *New J. Chem.*, **2020**, *44*, 8743-8750 ; b S. Zhang, J.-C. Xia, Z.-G. Wu, G.-Z. Lu, Y. Zhao, T.-X. Zheng, *Eur. J. Inorg. Chem.*, **2016**, 2556-2561; c) G. Ge, J. He, H. Guo, F. Wang, D. Zou, *J. Organomet. Chem.*, **2009**, *19*, 3050-3057; d) B. H. Tong, Q. B. Mei, R. Q. Tian, M. Yang, Q. F. Hua, Y. J. Shi, S. H. Ye, *RSC. Adv.*, **2016**, *6*, 34970-34976; e) X.-F. Ma, J.-C. Xia, Z.-P. Yan, X.-F. Luo, Z.-G. Wu, Y.-X. Zheng, W.-W. Zhang, *J. Mater. Chem. C*, **2019**, *7*, 2570-2576; f) W.-K. Hu, S.-H. Li, X.-F. Ma, S.-X. Zhou, Q.-F. Zhang, J.-Y. Xu, P. Shi, B.-H. Tong, M.-K. Fung, L. Fu. *Dyes Pigm.*, **2018**, *150*, 284-292.

[13] a) M. Z. Shafikov, S. Tang, C. Larsen, M. Bodensteiner, V. N. Kozhevnikov, L. Edman, *J. Mater. Chem. C*, **2019**, *7*, 10672-10682; b) C. Damm, G. Israel, T. Hegmann, C. Tschierske, *J. Mater. Chem.*, **2006**, *16*, 1808-1816.

[14] N. Miyaura, A. Suzuki, *Chem. Rev.*, **1995**, *95*, 2457-2483.

[15] a) A. F. Littke, G. C. Fu*, Angew. Chem. Int. Ed.*, **2002**, *41*, 4176-4211; b) S. Achelle, Y. Ramondenc, F. Marsais, N. Plé, *Eur. J. Org. Chem.*, **2008**, 3129-2140.

[16] A. C. Cope, R. W. Siekman, *J. Am. Chem. Soc.*, **1965**, *87*, 3272-3273.

[17] H. Fukudaa, Y. Yamadaa, D. Hashizumeb, T. Takayamac, M. Watabea, *Appl. Organometalic Chem.*, **2009**, *23*, 154–160.

[18] J. Kang, R. Zaen, K.-M. Park, K. H. Lee, J. Y. Lee,Y. Kang, *Cryst. Growth Des.*, **2020**, 20, 6129-6138.

[19] M. Taniguchi, J. S. Lindsey, *Photochem. Photobiol.*, **2018**, *94*, 290-327.

[20] (a) V. Barone, J. Bloino, M. Biczysko, F. Santoro, *J. Chem. Theo. Comp.*, **2009**, *5*, 540–554. (b) V. Barone, A. Baiardi, M. Biczysko, J. Bloino, C. Cappelli, F. Lipparini, *Phys. Chem. Chem. Phys.*, **2012**, *14*, 12404–12422.

[21] R. Schira, C. Latouche, *Dalton Trans.*, **2021**, *50*, 746-753.

[22] G. M. Sheldrick, *Acta Cryst.*, **2015**, *A71*, 3-8.

[23] G. M. Sheldrick, *Acta Cryst.*, **2015**, *C71*, 3-8.

[24] Gaussian 16, Revision B.01, M. J. Frisch, G. W. Trucks, H. B. Schlegel, G. E. Scuseria, M. A. Robb, J. R. Cheeseman, G. Scalmani, V. Barone, G. A. Petersson, H. Nakatsuji, X. Li, M. Caricato, A. V. Marenich, J. Bloino, B. G. Janesko, R. Gomperts, B. Mennucci, H. P. Hratchian, J. V. Ortiz, A. F. Izmaylov, J. L. Sonnenberg, D. Williams-Young, F. Ding, F. Lipparini, F. Egidi, J. Goings, B. Peng, A. Petrone, T. Henderson, D. Ranasinghe, V. G. Zakrzewski, J. Gao, N. Rega, G. Zheng, W. Liang, M. Hada, M. Ehara, K. Toyota, R. Fukuda, J. Hasegawa, M. Ishida, T. Nakajima, Y. Honda, O. Kitao, H. Nakai, T. Vreven, K. Throssell, J. A. Montgomery, Jr., J. E. Peralta, F. Ogliaro, M. J. Bearpark, J. J. Heyd, E. N. Brothers, K. N. Kudin, V. N. Staroverov, T. A. Keith, R. Kobayashi, J. Normand, K. Raghavachari, A. P. Rendell, J. C. Burant, S. S. Iyengar, J. Tomasi, M. Cossi, J. M. Millam, M. Klene, C. Adamo, R. Cammi, J. W. Ochterski, R. L. Martin, K. Morokuma, O. Farkas, J. B. Foresman, D. J. Fox, Gaussian, Inc., Wallingford CT, 2016.

[25] (a) J. P. Perdew, K. Burke, M. Ernzerhof, *Phys. Rev. Lett.*, **1996**, *77*, 3865-3868. (b) J. P. Perdew, K. Burke, M. Ernzerhof, *Phys. Rev. Lett.*, **1997**, *78*, 1396-1396. (c) C. Adamo, V. Barone, *J. Chem. Phys.*, **1999**, *110***,** 6158-6169.

[26] (a) T. H. Dunning Jr., P. J. Hay, in *Modern Theoretical Chemistry*, Ed. H. F. Schaefer III, Vol. 3 (Plenum, New York, 1977) 1-28; (b) P. J. Hay, W. R. Wadt, *J. Chem. Phys.*, **1985**, *82* 270; (c) W. R. Wadt, P. J. Hay, *J. Chem. Phys.*, **1985**, *82*, 284-298; (d) P. J. Hay, W. R. Wadt, *J. Chem. Phys.*, **1985**, *82*, 299-310.

[27] (a) M. Cossi, V. Barone, R. Cammi, J. Tomasi, *Chem. Phys. Lett.*, **1996**, *255*, 327-335. (b) V. Barone, M. Cossi, J. Tomasi, *J. Chem. Phys.*, **1997**, *107*, 3210-3221.

[28] S. I. Gorelsky, AOMix: program for molecular orbital analysis, *York University, Toronto*, 1997.

[29] E. D. Glendening, J. K. Badenhoop, A. E. Reed, J. E. Carpenter, J. A. Bohmann, C. M. Morales, F. Weinhold, 2013, NBO 6.0; Theoretical Chemistry Institute, University of Wisconsin, Madison, WI, http://nbo6.chem.wisc.edu.

[30] R. Dennington, T. Keith, J. Millam, K. Eppinnett, W. L. Hovell, R. Gilliland, GaussView, 2009.

[31] (a) V. Barone, J. Bloino, M. Biczysko, F. Santoro, *J. Chem. Theo. Comp.*, **2009**, *5*, 540–554. (b) V. Barone, A. Baiardi, M. Biczysko, J. Bloino, C. Cappelli, F. Lipparini, *Phys. Chem. Chem. Phys.*, **2012**, *14*, 12404–12422.

[32] (a) F. Santoro, R. Improta, A. Lami, J. Bloino, V. Barone, *J. Chem. Phys*., **2007**, *126*, 084509. (b) F. Santoro, A. Lami, R. I mprota, V. Barone, *J. Chem. Phys*., **2007**, *126*, 184102. (c) F. Santoro, A. Lami, R. Improta, J. Bloino, V. Barone, *J. Chem. Phys*., **2008**, *12*8, 224311.

[33] M. R. Kumar, K. Park, S. Lee, *Adv. Synth. Catalysis*, **2010**, *352*, 3255-3266.

[34] J.-M. Begouin, C. Gosmini, *J. Org. Chem.*, **2009**, *74*, 3221-3224.

[35] N. Plé, A. Turck, K. Couture, G. Quéguiner, *J. Org. Chem.*, **1995**, *60*, 3781-3786.